Gating-induced large aqueous volumetric remodeling and aspartate tolerance in the voltage sensor domain of Shaker K^+ channels

Ignacio Díaz-Franulic[a,b,c,1], Vivian González-Pérez[d], Hans Moldenhauer[a,b], Nieves Navarro-Quezada[a,b], and David Naranjo[a,1]

[a]Instituto de Neurociencia, Facultad de Ciencias, Universidad de Valparaíso, 2360102 Valparaíso, Chile; [b]Centro Interdisciplinario de Neurociencia de Valparaíso, Universidad de Valparaíso, 2360103 Valparaíso, Chile; [c]Center for Bioinformatics and Integrative Biology, Universidad Andrés Bello, 8370186 Santiago, Chile; and [d]Department of Anesthesiology, Washington University School of Medicine, St. Louis, MO 63110

Edited by Richard W. Aldrich, The University of Texas at Austin, Austin, TX, and approved June 26, 2018 (received for review April 25, 2018)

Neurons encode electrical signals with critically tuned voltage-gated ion channels and enzymes. Dedicated voltage sensor domains (VSDs) in these membrane proteins activate coordinately with an unresolved structural change. Such change conveys the transmembrane translocation of four positively charged arginine side chains, the voltage-sensing residues (VSRs; R1–R4). Countercharges and lipid phosphohead groups likely stabilize these VSRs within the low-dielectric core of the protein. However, the role of hydration, a sign-independent charge stabilizer, remains unclear. We replaced all VSRs and their neighboring residues with negatively charged aspartates in a voltage-gated potassium channel. The ensuing mild functional effects indicate that hydration is also important in VSR stabilization. The voltage dependency of the VSR aspartate variants approached the expected arithmetic summation of charges at VSR positions, as if negative and positive side chains faced similar pathways. In contrast, aspartates introduced between R2 and R3 did not affect voltage dependence as if the side chains moved outside the electric field or together with it, undergoing a large displacement and volumetric remodeling. Accordingly, VSR performed osmotic work at both internal and external aqueous interfaces. Individual VSR contributions to volumetric works approached arithmetical additivity but were largely dissimilar. While R1 and R4 displaced small volumes, R2 and R3 volumetric works were massive and vectorially opposed, favoring large aqueous remodeling during VSD activation. These diverse volumetric works are, at least for R2 and R3, not compatible with VSR translocation across a unique stationary charge transfer center. Instead, VSRs may follow separated pathways across a fluctuating low-dielectric septum.

voltage sensor | charge hydration | osmotic work | conformational change | Shaker

Voltage-dependent K^+ (Kv) ion channels are membrane proteins involved in a myriad of physiological processes exquisitely regulated by membrane potential (1–4). By allowing the permeation of potassium ions, they drive the membrane voltage toward the K^+ equilibrium potential, modulating cell excitability (5). Assembled as tetramers, each Kv channel subunit has six transmembrane segments (S1–S6), of which S1–S4 constitute the voltage sensor domain (VSD) and S5 and S6, placed at the channel fourfold symmetry axis, form the ion conduction pathway (6). In Shaker Kv channels, voltage sensitivity is mostly due to the electrophoretic transmembrane migration of four arginine residues [voltage-sensing residues (VSRs); R1–R4] placed in VSD's S4 (7–10). The total charge displaced per channel for the native Shaker is 12–13 e_0, while for the R2Q, R3N, and R4Q variants, it is about three-quarters of the total (8, 9). These amounts agreed with the measures of the electrical valence of the voltage dependence of pore opening (Z). Thus, almost all of the charge movement is used to open the ion conduction pore (8). This concept applies to other Kv, Cav, and Nav ion channels also (2, 4, 11).

Because charged particles are energetically disfavored in the low-dielectric membrane environment, electrostatic stabilization of VSR should occur through contacts with negative side chains in the protein core and/or lipid phosphohead groups (12–16). Because these charge stabilization mechanisms are sign-specific, charge reversions in VSR should lead to dramatic alteration of the VSD structure. We performed an aspartate scanning along the S4 region hosting R1–R4 of the Shaker K^+ channel. Because all aspartate variants displayed moderate functional alterations, sign-independent VSR charge stabilization mechanisms as hydration must exist. Then, VSD activation implies water mobilization between compartments, such that we could expect osmotic work. By challenging the VSD with unilateral and bilateral hyperosmolarity, we found that each VSR contributes in a unique and vectorially different manner to the total osmotic work, perhaps across dissimilar trajectories.

Results

Sign-Independent Gating Charge Stabilization. We performed an aspartate scanning along the N-terminal half of S4 including all VSRs of Shaker (residues 359–371). Fig. 1*A* and *SI Appendix*, Fig. S1 show K^+-current traces for each aspartate-substituted

Significance

The neuronal action potential is a self-propagating transient depolarization traveling along the neuron membrane. This signal is produced by the coordinated activation of voltage-gated ion channels (VGCs), a family of ion-selective transmembrane proteins activated by depolarization. Sodium and calcium VGCs reinforce the signal, while potassium VGCs terminate it. A conserved voltage sensor domain (VSD) in VGCs responds with an unresolved conformational change driven by the transmembrane electrophoretic displacements of four arginine side chains. We show that those arginine side chains are stabilized by water impregnating the VSD and that, upon activation, displace large and dissimilar aqueous volumes at both protein faces. This charge translocation entails a transporter-like remodeling of water–protein interfaces that should create mechanical spikes accompanying action potentials.

Author contributions: I.D.-F., V.G.-P., H.M., and D.N. designed research; I.D.-F., V.G.-P., H.M., and D.N. performed research; I.D.-F., V.G.-P., H.M., N.N.-Q., and D.N. contributed new reagents/analytic tools; I.D.-F., V.G.-P., and D.N. analyzed data; and I.D.-F. and D.N. wrote the paper.

The authors declare no conflict of interest.

This article is a PNAS Direct Submission.

[1]To whom correspondence may be addressed. Email: david.naranjo@uv.cl or ignacio.diaz@cinv.cl.

This article contains supporting information online at www.pnas.org/lookup/suppl/doi:10.1073/pnas.1806578115/-/DCSupplemental.

Published online July 23, 2018.

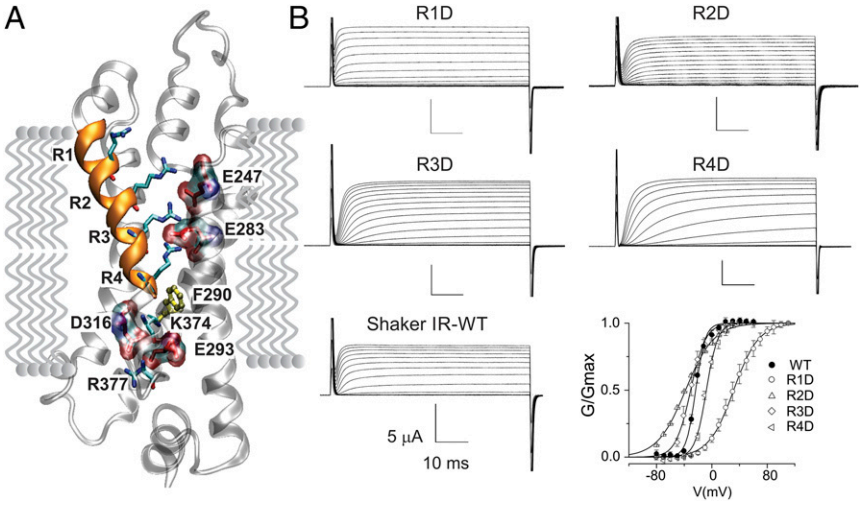

Fig. 1. Shaker Kv variants with Asp-substituted VSR. (*A*) The voltage sensor of the N290R-Kv1.2–2.1 paddle chimera (Protein Data Bank ID code 2R9R) with Shaker residue numbering. The region encompassing S1–S3 is in gray, and S4, including the VSRs, is gold. VSRs R362, R365, R368, and R371 are labeled R1–R4; acidic residues (E247, E283, E293, and D316) in S1–S3 are transparent volumes. F290, the putative charge transfer center, is in yellow. (*B*) Two-electrode voltage clamp recordings of Asp-substituted VSR responding to 50-ms voltage pulses. *G–V* curves of WT channels (black circles), R1D (white circles), R2D (triangles), R3D (diamonds), and R4D (left-rotated triangles). Continuous lines are Boltzmann function fits with parameters for WT: $V_{1/2}$ = –23.3 ± 1.1, z = 3.7 ± 0.3 (n = 4); R1D: $V_{1/2}$ = 32.1 ± 1.9, z = 1.4 ± 0.1 (n = 7); R2D: $V_{1/2}$ = –38.4 ± 1.0, z = 1.3 ± 0.1 (n = 7); R3D: $V_{1/2}$ = –28.7 ± 4.3, z = 2.6 ± 0.3 (n = 6); and R4D: $V_{1/2}$ = –7.8 ± 1.6, z = 3.1 ± 0.5 (n = 7).

variant either on the native VSR arginine (Fig. 1) or on uncharged inter-VSR positions (*SI Appendix*, Fig. S1) in response to voltage pulse protocol. Fig. 1*B* and *SI Appendix*, Fig. S1 show the calculated conductance as a function of the applied voltage (*G–V*) (*Materials and Methods*). Considering the high conservation, the scrutinized region was very tolerant to aspartate, a replacement that, in most cases, constituted a chemically drastic change. Neighboring pairs 363D/364D and 369D/370D (*SI Appendix*, Fig. S1) have their *G–V* relationships almost superimposed, while 366D/367D are ∼80 mV apart. Compared with *wt* channels, only one variant (367D) showed a *G–V* relationship shifted <60 mV, corresponding roughly to an energy impact of <16 kJ/mol per subunit, which is comparable with the break/formation of one to three hydrogen bonds. Consistent with these results, with Network Enthalpic Modelling (NeEMO), a method using residue interaction network to calculate the energy impact of each mutation on the structure, we observed that all impacts were <9.5 kJ/mol (17) (*Materials and Methods* and *SI Appendix*, Fig. S2). In comparison, the expected charge reversion penalty in protein ion pairs is higher (25–100 kJ/mol) (18). These extremely moderate effects argue in favor of a structurally robust design for the VSD and sign-independent charge stabilization of VSRs.

To test if the aspartate side chains behave as the native VSR arginine, we measured Z, with the limiting slope method, to all 10 Asp variants encompassed by R1–R4. We recorded the activity of hundreds or thousands of channels in inside-out membrane patches at voltages negative enough so that the open probability (*Po*) is $<10^{-4}$ (*Materials and Methods*) (19). Thus, openings correspond to channels that traveled most of the activation pathway in a single excursion, revealing the entire voltage dependency. For Shaker and other Kv, Cav, and Nav channels, Z approximates correctly to the total charge movement (1–4, 8, 11).

Fig. 2 *A–C* summarizes the procedure for Z measurements to the R365D variant (R2D). Fig. 2*A* shows representative 10-s segments taken from 5-min recordings of a membrane patch having ∼100 channels at different applied voltages. The apparent *Po* (*N*·*Po*, with *N* = number of channels) is the fraction of the time that a channel is detected as active (*Materials and Methods*). We used the nonstationary noise analysis method to find *N* of the same membrane patch shown in Fig. 2*A* (Fig. 2*B*) (3, 20). The relationship between the average trace of hundreds of K^+-current relaxations (Fig. 2*B*, middle trace) and the total variance among traces (Fig. 2*B*, lower trace) is an inverted parabola with roots in zero and *Ni*, with *i* being the unitary amplitude (Fig. 2*B*, *Inset*). For R2D, *Po* approached ∼3 × 10^{-5} at −135 mV (Fig. 2*C*), growing e-fold every 4.2 mV, which yields Z = 6.1 (3), Fig. 2*D* shows a summary of the Asp scanning results within R1–R4.

Most Asp substitutions decreased Z. In VSR positions, decreases were to 39–70% (Fig. 2*D*, white bars). For R2D and R3D, Z is ∼50%, an outcome consistent with arithmetic charge additivity in S4 ($3R^+ + 1D^- = +2$). Thus, these aspartate side chains may follow similar paths across the electric field as the native arginine. However, R1D and R4D depart from such arithmetic expectancy, suggesting additional electric field and/or structural remodeling in these mutants. Still, this outcome strongly argues for the existence of a sign-independent VSR stabilization within the VSD.

Substitutions in the hydrophobic inter-VSR positions showed significant reduction in Z toward the R1 and R4 ends and minimal effects between R2 and R3 (Fig. 2*D*, gray bars). We previously proposed that the Z reduction in 363D and 364D is due to inward displacements of the external electric-field boundaries, leaving at

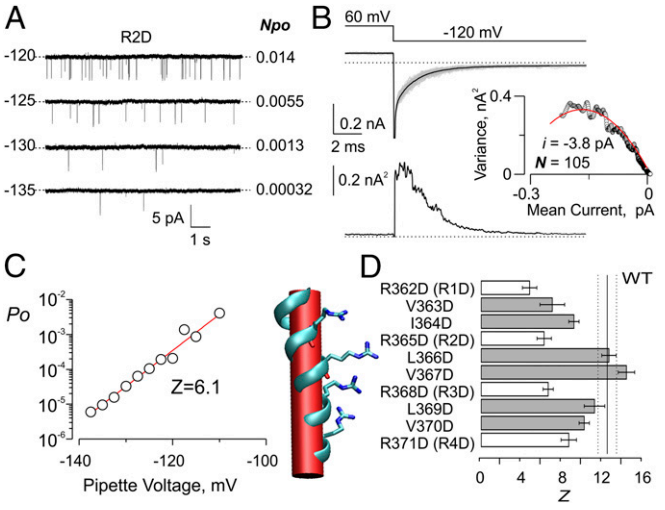

Fig. 2. Limiting slope Z determination for Asp scanning. (*A*) Single-channel segments representative of 5-min recordings of a membrane patch having ∼100 Shaker R365D channels (R2D). Openings are downward, and the voltage and *NPo* are shown at the right and left of each trace, respectively. The dotted lines mark the zero current levels. (*B*) Channel counting. (*Upper*) Mean relaxation (in black) of 110 individual traces (in gray) from the patch shown in *A*; *Lower* is the time course of the variance, and *Inset* is the mean vs. variance plot. The continuous line is the fit of $\mathrm{Var} = i \cdot I + I^2/N$, where *I* is mean current, *i* is unitary amplitude, and *N* is the number of channels (3, 20). (*C*) Absolute *Po* (*NPo*/*N*) plotted vs. voltage for the patch recordings in *A* and *B*. The continuous line is an exponential growth function, with *Po* increasing e-fold every 4.4 mV (*Z* = 6.1). (*D*) Summary of Z of Asp substitutions in S4. Data from *wt*, V363D, and I364D are from refs. 2 and 3; n = 3–4 patches for all variants.

least R1 eternally outside (3). We guess that the Z reduction for 370D could also result from electric-field remodeling, perhaps produced by outward displacement of its cytosolic boundaries, increasing 370D and R4 internal exposure. In contrast, 366D and 367D, between R2 and R3, show minimal effects in Z, suggesting either a physical trajectory outside or "together with" the electric field. Because current activation models propose that S4 moves 7–15 Å vertically (21–23), if the septum separating the internal and external faces moves together with 366D/367D, we should expect a substantial activation-related volumetric remodeling of the VSD, implying significant osmotic work.

Osmotic Work at the VSD. If VSD activation produces a change in solute-inaccessible aqueous volume, in hyperosmolar conditions it should perform additional osmotic work. Thus, the net free energy change of the VSD activation (ΔG) is the conformational energy difference plus the osmotic and electric works:

$$\Delta G = \Delta G_0 + \Pi \Delta \nu - zFV, \quad [1]$$

where ΔG_0 is the standard conformational free energy difference between resting and active VSDs, Π is the recording solution osmotic pressure, $\Delta\nu$ is the fluctuation in solute-inaccessible aqueous volume, z is charge equivalent mobilized during activation, F is the Faraday constant, and V is the applied voltage. The negative sign in the electrical term specifies that positive voltages favor the active conformation. Because VSD activation implies the movement of charge in response to a voltage pulse, such charge rearrangement is detected as transient, nonlinear, nonionic currents in the membrane patch "gating currents" (24) (Fig. 3*A*). By integrating the "On" gating currents (Fig. 3*A*, *Inset*), we measured the relative charge displaced by the VSD (Q) as a function of the voltage (Q–V) (Fig. 3*B*). The voltage at which the active and resting conformations are equally populated ($\Delta G = 0$) is the median voltage, V_M (25). Then, zFV_M offers an estimation of the transition net free energy difference. To raise the osmotic pressure ($\Delta\Pi$), we added sucrose to the recording solutions. Then, the extra work performed by the VSD in this hypertonic challenge is perceived as a shift in V_M (ΔV_M). Thus, the volumetric change per 1 mole of VSD ($\Delta\nu$) is

$$\Delta\nu = \frac{z \cdot F \cdot \Delta V_M}{\Delta\Pi}. \quad [2]$$

There are two practical considerations to contemplate. On one hand, in voltage-gated ion channels, the main conformational changes are related to the pore-opening transitions, concealing those of the VSD (26). On the other hand, the gating currents are visible after pharmacological or genetical removal of the channel's ionic conductance. To circumvent both difficulties, we used a nonconductive, constitutively closed Shaker variant, Shaker-V478W (V478W) (27). V478W should minimize pore-related osmotic work, because the 478-tryptophan side chains form a hydrophobic plug, preventing the inner gate pore opening (27). Fig. 3*A* shows gating currents traces from V478W and individually VSR-neutralized variants in control recording solution (Fig. 3*A*, black traces) and with additional bilateral 2 M sucrose to raise osmotic pressure by $\Delta\Pi \sim cRT \sim 5$ kJ/L (*Sym-Suc*) (Fig. 3*A*, blue traces). For V478W (*wt*), $\Delta V_M = 8 \pm 2$ mV, indicating that symmetric hypertonicity modestly disfavored the active VSD (Fig. 3*B* and Table 1). To apply Eq. **2**, we need to know z, which according to several groups and methods, is 12–13.6 e_0 for the WT tetrameric channel (1, 3, 8, 9). Because each VSD in Shaker acts independently, we took $z = 0.25 \times 13.3$ e_0 (9). Thus, $zF\Delta V_M = 2.63 \pm 0.65$ kJ/mol, corresponding, according to Eq. **2**, to $\Delta\nu = 0.53 \pm 0.13$ L/mol. Because 1 L holds ~55 mol of water, such increment equals 29 ± 7 water molecules per VSD. Then, the active *wt*-VSD grows a net $\geq 870 \pm 210$-Å^3 solvent-filled cavity. This volume is 20–60% of that estimated for pore opening (26, 28). Because we expected large septum displacements, such modest volumetric outcome may result from larger and vectorially opposite osmotic works by the VSD.

Volumetric Work of the VSR Variants. We neutralized R1–R4 individually to distinguish their specific volumetric work and to conceive their hydration landscape during activation (Fig. 3). In *Sym-Suc*, R1N and R2Q showed shifts of +15 and +30 mV, respectively (Table 1), which with $z = 2.3$ and 2.1 e_0, represent gains of 36 and 66 waters, respectively. In contrast, R3N showed a negative shift (-13 ± 3 mV) that, with $z = 2.5$ e_0, meant a net loss of 34 waters, while R4Q showed no significant shift in the V_M. Interestingly, these results differ in size and sign among variants, suggesting that VSRs behave distinctively in terms of volumetric work.

To identify which interfaces, internal or external, exchange water with the VSD, we exposed the VSR variants to unilateral hypertonic trials. Fig. 4*A* shows the gating currents of all V478W variants exposed to internal (Fig. 4*A*, red traces, *In-Suc*) or external (Fig. 4*A*, green traces, *Ex-Suc*) hyperosmotic recording solutions. Again, the Q–V relationships showed distinctive behavior for all variants. In V478W, high internal sucrose produced a negligible $\Delta V_M = 5 \pm 3$ mV, while in external hypertonicity, it produced a $\Delta V_M = 11 \pm 3$ mV, indicating larger external volumetric work (Table 1). Signifying that R1 acts mostly at the external face, R1N was only responsive to internal hyperosmolarity. R2Q and R3N showed consistently large and opposite sensitivities in all conditions, revealing operation at both interfaces. Because R4Q was unresponsive to internal hypertonicity, R1 should work at the cytosolic face only. Thus, the VSRs must experience different hydration paths during activation.

Individual Contributions of VSRs to the Volumetric Work. We assumed that the individual volumetric works added linearly to outline the total VSD work. This assumption rests on that most

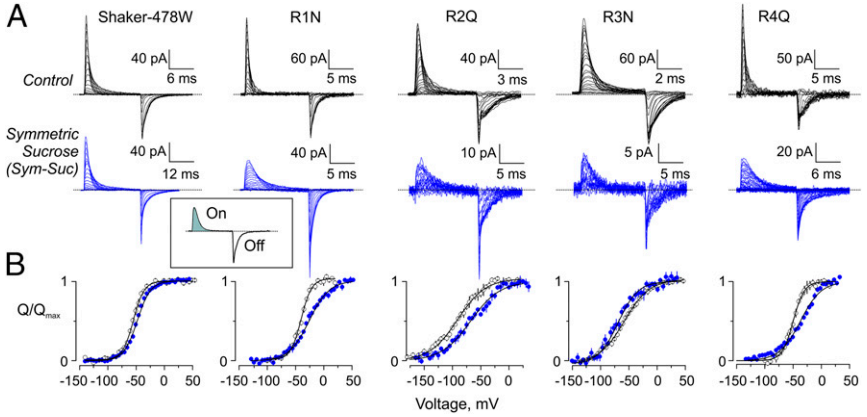

Fig. 3. Gating currents in high symmetrical osmolarity. (*A*) Representative recordings of gating currents in control (black traces) and in hypertonic solution (*Symmetric Sucrose* in blue traces). The variants are Shaker-V478W (*wt*), V478W/R362N (R1N), V478W/R365Q (R2Q), V478W/R368N (R3N), and V478W/R371Q (R4Q). The current traces were evoked by voltage pulses ranging from −220 to 50 mV (a detailed protocol description is in *SI Appendix*, Fig. S4). (*Inset*) The charge, Q, was the integral of the current at the On. (*B*) Average Q–V relations in normoosmotic (white symbols) and hypertonic recording solution (blue symbols). Solid lines are Boltzmann fits. Fit parameters are in *SI Appendix*, Table S2.

Table 1. Estimation of the differential volumetric work by VSR variants

Variant	V478W (*wt*)	R1N	R2Q	R3N	R4Q
Control V_M, mV	−59 ± 1 (n = 7)	−46 ± 3 (n = 6)	−95 ± 3 (n = 6)	−58 ± 2 (n = 6)	−50 ± 3 (n = 5)
Sym-Suc V_M, mV	−51 ± 2 (n = 4)	−31 ± 2 (n = 4)	−65 ± 5 (n = 3)	−71 ± 3 (n = 4)	−48 ± 3 (n = 6)
ΔV_M, mV	8 ± 2	15 ± 3	30 ± 6	−13 ± 3	2 ± 4
$\Pi\Delta\nu$, kJ/mol	2.63 ± 0.65	3.28 ± 0.71	5.97 ± 1.17	−3.10 ± 0.77	0.52 ± 0.79
$\Delta n_{W\text{-}Var}$	29 ± 7	36 ± 8	66 ± 13	−34 ± 9	6 ± 9
In-Suc V_M, mV	−54 ± 2 (n = 7)	−32 ± 2 (n = 4)	−70 ± 3 (n = 4)	−76 ± 5 (n = 4)	−51 ± 3 (n = 3)
ΔV_M, mV	5 ± 3	14 ± 4	25 ± 4	−19 ± 5	−1 ± 3
$\Pi\Delta\nu$, kJ/mol	1.60 ± 0.81	3.23 ± 0.81	4.97 ± 0.81	−4.39 ± 1.19	−0.13 ± 0.78
$\Delta n_{W\text{-}Var}$	18 ± 9	36 ± 9	55 ± 9	−49 ± 13	−1 ± 9
Ex-Suc V_M, mV	−47 ± 2 (n = 8)	−51 ± 0.3 (n = 3)	−61 ± 1 (n = 7)	−65 ± 2 (n = 7)	−37 ± 3 (n = 4)
ΔV_M, mV	11 ± 3	−5 ± 3	34 ± 3	−7 ± 3	14 ± 3
$\Pi\Delta\nu$, kJ/mol	3.63 ± 0.82	−1.12 ± 0.63	6.67 ± 0.64	−1.73 ± 0.73	3.03 ± 0.74
$\Delta n_{W\text{-}Var}$	40 ± 9	−12 ± 7	75 ± 7	−19 ± 8	34 ± 8

The differential volumetric work performed by all variants (*wt* and *Mut*) was calculated from Eq. **2**, with z taken as 1/4 of the charge per channel (1): 3.3, 2.3, 2.1, 2.5, and 2.3 e_0 for V478W (*wt*), R1N, R2Q, R3N, and R4Q, respectively. Δn_W is the change in solvent-exposed volume (in water molecules) associated with activation of each variant. The number of experiments is in parentheses.

charge reversions or neutralizations in Shaker VSR contributed in roughly linear fashion to the voltage dependence (Fig. 2*D*) (8, 9, 29). For this assumption to be meaningful, the VSD must preserve its structural integrity across the mutations (the mutations act locally), so that the transitional ΔG is conservative (30). Then, the total V478W VSD volumetric work should equal the sum of the individual VSR contributions. We developed two distinct methods to compute individual volumetric works (Table 2). In the first method, the contribution of the absent arginine ($W_{Osm|-R}$) is the osmotic work of V478W minus the work of the variant missing the specified VSR (*wt-relative*). Thus,

$$W_{Osm|-R} = \left(\Delta G_{wt|Suc} - \Delta G_{wt}\right) - \left(\Delta G_{Mut|Suc} - \Delta G_{Mut}\right), \qquad [3]$$

where $\Delta G_{wt|Suc} - \Delta G_{wt} = z_{wt}F\Delta V_M$ for V478W channels and $\Delta G_{Mut|Suc} - \Delta G_{Mut} = z_{Mut}F\Delta V_m$ for the variants. The second method finds the individual contributions from the linear combination of the four variants' osmotic works (excluding V478W) in a linear four-equation system. Eq. **4** shows an example of this method (in water molecules) applied to the symmetric sucrose results of Table 1, fifth row:

$$\left.\begin{array}{ll} \text{R1N:} & \text{R2}+\text{R3}+\text{R4} = \ 36\pm8 \\ \text{R2Q:} & \text{R1}+\text{R3}+\text{R4} = \ 66\pm13 \\ \text{R3N:} & \text{R1}+\text{R2}+\text{R4} = -34\pm9 \\ \text{R4Q:} & \text{R1}+\text{R2}+\text{R3} = \ \ 6\pm9 \end{array}\right\}. \qquad [4]$$

Table 2 shows the volumetric work of each VSR calculated with the *wt-relative* and linear combination methods (Eqs. **3** and **4**, respectively). For all osmotic tests, there is a good agreement between results from both methods (Fig. 5*A*). This correlation, which theoretically, should be 1:1 (Fig. 5*A*, dotted red line), validates these two analytical methods as readouts of a conservative transitional ΔG. Similar data correspondence was found using z estimates from the laboratory of Bezanilla and coworkers (8) and from our own Boltzmann fits (*SI Appendix*, Fig. S3 and Table S2). Furthermore, with both methods, the summation of the VSR volumetric works is close to *wt* in most cases (compare R1 + R2 + R3 + R4 with *wt* in Table 2). Having in mind that mutations in S4 possibly altered the VSD structure and/or the physical trajectory of each VSR, the fact that, with both methods (Eqs. **3** and **4**), we can arrive reasonably well to the osmotic behavior of the native VSD from the combined results of the mutants is not consistent with global unpredicted structural modifications of the VSD (30, 31). In addition, the total osmotic work seems to arise from the VSRs solely, validating our choice of the V478W Shaker variant as the background to address the VSD volumetric changes.

In contrast to the approximately equivalent contributions to the electrical work, our results suggest that VSR osmotic works are different: for R1, it is small, except for *Ex-Suc*, in which a prominent amount of water is gained (Fig. 5 *A* and *B*). R2 loses ∼45 waters, while R3 gains ∼60 waters in all scenarios. Finally, R4 gains ∼20 waters from the cytosolic face. The small sensitivity of R1 and R4 to internal and external sucrose, respectively, suggests that they do not cross the membrane entirely, in agreement with methane–sulfonate accessibility (7, 10). Unilateral and bilateral osmolarity tests suggest that R2 associates with

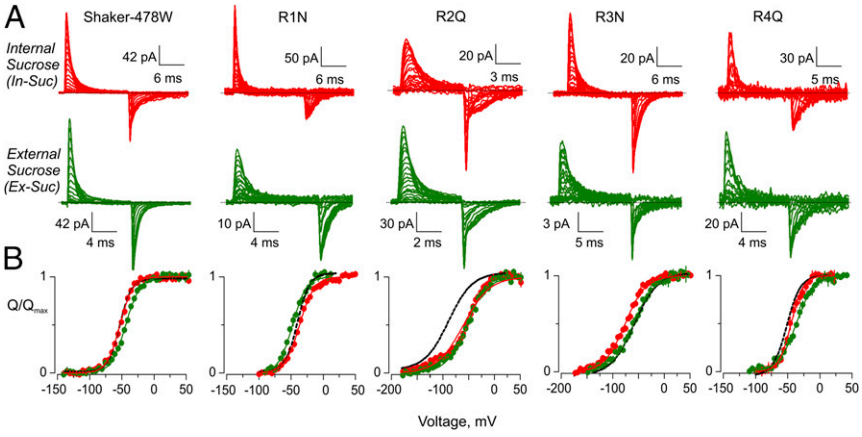

Fig. 4. Gating currents in high asymmetrical osmolarity. (*A*) Representative traces of gating currents of Shaker-V478W variants. Voltage pulses are depicted in *SI Appendix*, Fig. S4. (*B*) Average *Q–V* relations for each variant (same color code as the recording panels). Dotted black curves are Boltzmann fits for the corresponding variant in control conditions shown for reference. Fit parameters are in *SI Appendix*, Table S2.

Table 2. Individual volumetric work of each VSR

Method	VSR					
	R1	R2	R3	R4	R1 + R2 + R3 + R4	*wt*
Sym-Suc						30 ± 7
wt-relative (Eq. **3**)	−7 ± 11	−37 ± 15	64 ± 11	23 ± 11	43 ± 24	
Linear combination (Eq. **4**)	−11 ± 8	−41 ± 10	59 ± 8	19 ± 8	25 ± 17	
In-Suc						18 ± 9
wt-relative (Eq. **3**)	−18 ± 13	−37 ± 13	66 ± 16	19 ± 13	30 ± 27	
Linear combination (Eq. **4**)	−22 ± 9	−41 ± 9	63 ± 10	15 ± 9	14 ± 19	
Ex-Suc						41 ± 9
wt-relative (Eq. **3**)	53 ± 11	−35 ± 12	59 ± 12	7 ± 12	84 ± 24	
Linear combination (Eq. **4**)	38 ± 6	−49 ± 7	45 ± 7	−8 ± 6	26 ± 13	

Calculations of individual volumetric work from data in Table 1. To assess uncertainties propagation, we assumed uncorrelated experimental errors. For the *wt-relative* (Eq. **3**), error for each VSR was $\sigma^2_{VSR} = \sigma^2_{Var} + \sigma^2_{wt}$, in which σ_{VSR}, σ_{Var}, and σ_{wt} are the SDs for each VSR, VSR variant, and V478W, respectively. For the linear combination (Eq. **4**), we estimated the VSR errors by iterative perturbations introduced into the equation system. Every time, the equation system turned different results for VSR, which were compared with the solutions. The resulting variations for each VSR were then added as $\sigma^2_{VSR} = \sigma^2_{R1} + \sigma^2_{R2} + \sigma^2_{R3} + \sigma^2_{R4}$ (46).

cytosolic solvent at resting and internally releases 40–56 waters while moving across the membrane, while R3 releases 50–68 water molecules to the external side. Thus, R2 and R3 perform vectorially opposed volumetric works equivalent to the internal collapse and external formation of 1,400- to 2,000-Å^3 aqueous cavities. Surprisingly, R1 shows no change in hydration in *Sym-Suc* and *In-Suc* but shows a gain of 43–53 waters (1,300–1,600 Å^3) in *Ex-Suc*. Not understanding the cause for such discrepancy, we speculate that the asymmetric osmotic stress created by the external hypertonicity produces water effluxes that, on VSD activation, locally dilute the external sucrose near R1. Fig. 5*C* pictorially represents these conclusions, where the movements of R2 and R3 (and R1 to a lesser extent) produce a vast change in aqueous exposure along with electric-field remodeling.

Discussion

S4 Conservation May Not Be Structurally Constrained. Most S4 residues in Kv channels are either conserved, as the hydrophobic ones, or highly conserved, as the VSRs (32). Thus, the mild functional consequences of the Asp substitutions and the nearly linear volumetric works discussed above reveal the VSD as a highly robust structure that stands chemically dramatic substitutions. In fact, VSD shows structural invariance in numerous experimental conditions: either isolated in different lipid families or attached to alien pore domains (21, 33–35). Such robustness may stem from a diversity of VSR stabilizing mechanisms, such as lipid and protein countercharges (13–15, 22). We show here that sign-independent mechanisms, such as hydration, are also central (Figs. 1 and 2). Having such diverse structurally preserving mechanisms, we suggest that sequence conservation in the external half of S4 is not ruled by VSD structural constrains. In fact, S4 residue variability in Kv channels is uncorrelated with the sequence anywhere else in the protein (32). Instead, S4 conservation could be driven by functional fine tuning with other voltage-gated proteins for correct electrical signal encoding. A good example of this fine tuning is that the hydrophilicity of residues in S2 and S4 controls Nav channels kinetics so that its activation precedes that of Kv channels, an essential requirement to generate action potentials (36).

The Volumetric Remodeling of the VSD During Activation. With current structural models for active and resting VSD and with the help of molecular dynamics simulations, voltage-dependent gating had amalgamated into a syncretic view in that VSRs move across a charged network of electrostatic interactions with acidic side chains in S1–S3 (8, 13, 16, 21, 22) and phospholipids (14, 15). Voltage pushes VSRs across several aromatic and hydrophobic residues that shape a short hydrophobic plug, or charge transfer center, near F290 (Fig. 1*A*). VSD activation should occur in approximately four small steps or clicks of 5–7 Å (37, 38). The hydrophobic plug may separate two aqueous compartments, forming the short septum defined by methane–sulfonate accessibility (29). Thus, it is surprising that residues L366D/V367D, flanked by R2–R3, which move across the entire electric field and are responsible for the largest volumetric change, do not affect Z. Then, L366D/V367D must move outside the electric field and together with the septum, cover a considerable physical distance. Hydrated 366D and 367D side chains should be constitutively exposed to the external and internal interfaces, respectively, producing the electrostatic biases of −20 and +60 on their respective *G–V* relationships (*SI Appendix*, Fig. S1).

Our osmotic results are in agreement with the overall VSR changes in solvent accessibility during Shaker and in other VSD proteins activation (7, 10, 39, 40). The large water numbers that we found surpass arginine hydration numbers by 5- to 10-fold, being instead comparable with the volume of the channel's pore cavity, ~1,600 Å^3 (41–43). Thus, our numbers probably represent conformational changes linked to the VSRs movement. R2 movement vanishes an ~1,500- to 3,000-Å^3 internal compartment on activation, while R3 shapes a similarly sized external

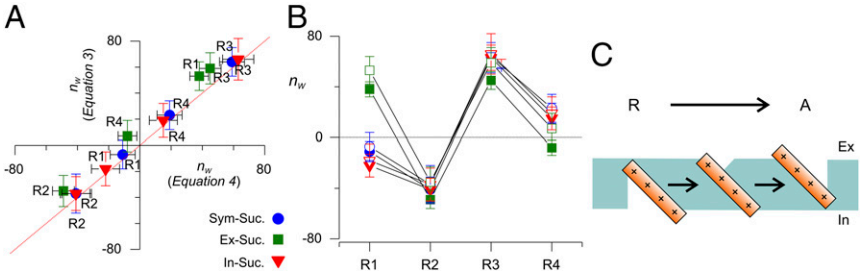

Fig. 5. Volumetric work of the VSR. (*A*) Comparison between volumetric work for individual VSRs estimated with the "*wt-relative*" (Eq. **3**) and "linear combination" (Eq. **4**) methods. The straight dotted line is the ideal relation between both methods (with a slope of one and intercept at the origin). (*B*) Volumetric work for individual VSR for Eq. **3** (open symbols) and Eq. **4** (filled symbols). (*C*) Cartoon summarizing the results. A large aqueous vestibule vanishes when R2 becomes internally inaccessible, and a large vestibule is created after R1 and R3 get exposed extracellularly with a small net vertical movement of S4.

compartment in the active VSD. By moving perpendicular to the membrane plane, VSR, mostly R2 and R3, drags inwardly relative to VSRs, the boundaries of the hydrophobic septum (and of the electric field). Such movement could be a rotation along the axis of the inclined α-helical S4 segment (Fig. 5*C*), with 366 and 367 side chains being dragged inwardly while R2 and R3 move outward, respectively. Then, the charge transfer center behaves as a dynamic structure during VSD activation, in which R2 and R3 sense different molecular landscapes. This conclusion is in line with structural interpretations that compare VSD activation with transporter conformational change (21, 44) but contradicts molecular calculations suggesting stable electric field among different VSD structures (23).

By inward dragging the hydrophobic septum together with S4's outward activation movement, the Kv channel VSD would make a volumetric work that should produce cell swelling. Considering that we underestimate the enlargement, because it considers only sucrose-excluding compartments, in a 5-μm-radius spherical cell with a density of ∼3,000 Nav, Kv, and Cav channels per 1 μm^2, an action potential would produce a >1-Å transient radial cell swelling. This interpretation provides a molecular sustentation for the observed mechanical spikes associated with action potentials (45).

Materials and Methods

Site-Directed Mutagenesis, Channel Expression, and Electrophysiology. All Shaker mutant stems from Shaker B (Δ64–6) were generated as before (3, 43).

Limiting Slope and Gating Currents. Limiting slope and gating currents recordings were performed with the patch clamp technique in inside-out configuration with an Axopatch 200B amplifier through a Digidata 1440 interface under control of pClamp 10 (Molecular Devices). For limiting slope recording, the pipette solution had 110 mM potassium methanesulfonate, 2 mM $CaCl_2$, and 10 mM Hepes, pH 7.4, with $CaCl_2$ being replaced by $MgCl_2$ in the bath solution. Gating currents recording solution contained 100 mM *N*-methyl-D-glucamine, 5 mM EGTA, 2 mM KCl, and 10 mM Hepes, pH 7.4. The two-electrode voltage clamp recording solution contained 100 mM NaCl, 2 mM KCl, 2 mM $CaCl_2$, 1 mM $MgCl_2$, and 10 mM Hepes-NaOH, pH 7.4. Recordings were performed with an OC-725C amplifier (Warner Instruments) through a PCI-6035 interface (National Instruments) running WinWCP (Strathclyde University). All experiments were at room temperature (22 °C to 24 °C).

Data Analysis. Analysis was done with Clampfit 10. To compute conductance vs. voltage (*G–V*) relations, current amplitude measured at the end of the test voltage pulse was divided by the K^+ driving force, assuming a reversal potential of −100 mV. Offline analyses of single-channel activity were as before (3). The On phase of the gating currents was integrated, after correcting for leak, to construct the *Q–V* relations. The median voltage V_M was calculated by the trapezoid rule, with a custom-made Excel routine (25). Additional experimental details and analysis are in *SI Appendix, SI Methods*.

ACKNOWLEDGMENTS. We thank Chris Lingle and Yu Zhou (Washington University) for critical reading of the manuscript and Victoria Prado for *Xenopus* care and oocyte preparation. We also thank Millennium Scientific Initiative P029-022-F. This work was supported by Fondecyt Postdoctoral Grants 3170599 (to I.D.-F.) and 3160321 (to H.M.).

1. Islas LD, Sigworth FJ (1999) Voltage sensitivity and gating charge in Shaker and Shab family potassium channels. *J Gen Physiol* 114:723–742.
2. Noceti F, et al. (1996) Effective gating charges per channel in voltage-dependent K+ and Ca2+ channels. *J Gen Physiol* 108:143–155.
3. González-Pérez V, Stack K, Boric K, Naranjo D (2010) Reduced voltage sensitivity in a K+-channel voltage sensor by electric field remodeling. *Proc Natl Acad Sci USA* 107:5178–5183.
4. Ishida IG, Rangel-Yescas GE, Carrasco-Zanini J, Islas LD (2015) Voltage-dependent gating and gating charge measurements in the Kv1.2 potassium channel. *J Gen Physiol* 145:345–358.
5. González C, et al. (2012) K(+) channels: Function-structural overview. *Compr Physiol* 2: 2087–2149.
6. Long SB, Tao X, Campbell EB, MacKinnon R (2007) Atomic structure of a voltage-dependent K+ channel in a lipid membrane-like environment. *Nature* 450:376–382.
7. Yang N, George AL, Jr, Horn R (1996) Molecular basis of charge movement in voltage-gated sodium channels. *Neuron* 16:113–122.
8. Seoh SA, Sigg D, Papazian DM, Bezanilla F (1996) Voltage-sensing residues in the S2 and S4 segments of the Shaker K+ channel. *Neuron* 16:1159–1167.
9. Aggarwal SK, MacKinnon R (1996) Contribution of the S4 segment to gating charge in the Shaker K+ channel. *Neuron* 16:1169–1177.
10. Larsson HP, Baker OS, Dhillon DS, Isacoff EY (1996) Transmembrane movement of the shaker K+ channel S4. *Neuron* 16:387–397.
11. Hirschberg B, Rovner A, Lieberman M, Patlak J (1995) Transfer of twelve charges is needed to open skeletal muscle Na+ channels. *J Gen Physiol* 106:1053–1068.
12. Papazian DM, et al. (1995) Electrostatic interactions of S4 voltage sensor in Shaker K+ channel. *Neuron* 14:1293–1301.
13. Tiwari-Woodruff SK, Schulteis CT, Mock AF, Papazian DM (1997) Electrostatic interactions between transmembrane segments mediate folding of Shaker K+ channel subunits. *Biophys J* 72:1489–1500.
14. Xu Y, Ramu Y, Lu Z (2008) Removal of phospho-head groups of membrane lipids immobilizes voltage sensors of K+ channels. *Nature* 451:826–829.
15. Schmidt D, Jiang QX, MacKinnon R (2006) Phospholipids and the origin of cationic gating charges in voltage sensors. *Nature* 444:775–779.
16. DeCaen PG, Yarov-Yarovoy V, Sharp EM, Scheuer T, Catterall WA (2009) Sequential formation of ion pairs during activation of a sodium channel voltage sensor. *Proc Natl Acad Sci USA* 106:22498–22503.
17. Giollo M, Martin AJ, Walsh I, Ferrari C, Tosatto SC (2014) NeEMO: A method using residue interaction networks to improve prediction of protein stability upon mutation. *BMC Genomics* 15(Suppl 4):S7.
18. Barlow DJ, Thornton JM (1983) Ion-pairs in proteins. *J Mol Biol* 168:867–885.
19. Almers W (1978) Gating currents and charge movements in excitable membranes. *Rev Physiol Biochem Pharmacol* 82:96–190.
20. Naranjo D, Wen H, Brehm P (2015) Zebrafish CaV2.1 calcium channels are tailored for fast synchronous neuromuscular transmission. *Biophys J* 108:578–584.
21. Li Q, et al. (2014) Structural mechanism of voltage-dependent gating in an isolated voltage-sensing domain. *Nat Struct Mol Biol* 21:244–252.
22. Vargas E, et al. (2012) An emerging consensus on voltage-dependent gating from computational modeling and molecular dynamics simulations. *J Gen Physiol* 140:587–594.
23. Souza CS, Amaral C, Treptow W (2014) Electric fingerprint of voltage sensor domains. *Proc Natl Acad Sci USA* 111:17510–17515.
24. Armstrong CM, Bezanilla F (1973) Currents related to movement of the gating particles of the sodium channels. *Nature* 242:459–461.
25. Chowdhury S, Chanda B (2012) Estimating the voltage-dependent free energy change of ion channels using the median voltage for activation. *J Gen Physiol* 139:3–17.
26. Zimmerberg J, Bezanilla F, Parsegian VA (1990) Solute inaccessible aqueous volume changes during opening of the potassium channel of the squid giant axon. *Biophys J* 57:1049–1064.
27. Kitaguchi T, Sukhareva M, Swartz KJ (2004) Stabilizing the closed S6 gate in the Shaker Kv channel through modification of a hydrophobic seal. *J Gen Physiol* 124:319–332.
28. Jiang X, Bett GC, Li X, Bondarenko VE, Rasmusson RL (2003) C-type inactivation involves a significant decrease in the intracellular aqueous pore volume of Kv1.4 K+ channels expressed in Xenopus oocytes. *J Physiol* 549:683–695.
29. Ahern CA, Horn R (2004) Specificity of charge-carrying residues in the voltage sensor of potassium channels. *J Gen Physiol* 123:205–216.
30. Hidalgo P, MacKinnon R (1995) Revealing the architecture of a K+ channel pore through mutant cycles with a peptide inhibitor. *Science* 268:307–310.
31. Schreiber G, Fersht AR (1995) Energetics of protein-protein interactions: Analysis of the barnase-barstar interface by single mutations and double mutant cycles. *J Mol Biol* 248:478–486.
32. Lee SY, Banerjee A, MacKinnon R (2009) Two separate interfaces between the voltage sensor and pore are required for the function of voltage-dependent K(+) channels. *PLoS Biol* 7:e47.
33. Lu Z, Klem AM, Ramu Y (2002) Coupling between voltage sensors and activation gate in voltage-gated K+ channels. *J Gen Physiol* 120:663–676.
34. Chakrapani S, Cuello LG, Cortes DM, Perozo E (2008) Structural dynamics of an isolated voltage-sensor domain in a lipid bilayer. *Structure* 16:398–409.
35. Krepkiy D, et al. (2009) Structure and hydration of membranes embedded with voltage-sensing domains. *Nature* 462:473–479.
36. Lacroix JJ, Campos FV, Frezza L, Bezanilla F (2013) Molecular bases for the asynchronous activation of sodium and potassium channels required for nerve impulse generation. *Neuron* 79:651–657.
37. Tao X, Lee A, Limapichat W, Dougherty DA, MacKinnon R (2010) A gating charge transfer center in voltage sensors. *Science* 328:67–73.
38. Lin MC, Hsieh JY, Mock AF, Papazian DM (2011) R1 in the Shaker S4 occupies the gating charge transfer center in the resting state. *J Gen Physiol* 138:155–163.
39. Villalba-Galea CA, Frezza L, Sandtner W, Bezanilla F (2013) Sensing charges of the Ciona intestinalis voltage-sensing phosphatase. *J Gen Physiol* 142:543–555.
40. Starace DM, Bezanilla F (2001) Histidine scanning mutagenesis of basic residues of the S4 segment of the shaker k+ channel. *J Gen Physiol* 117:469–490.
41. Zhao H (2006) Viscosity B-coefficients and standard partial molar volumes of amino acids, and their roles in interpreting the protein (enzyme) stabilization. *Biophys Chem* 122:157–183.
42. Moldenhauer H, Díaz-Franulic I, González-Nilo F, Naranjo D (2016) Effective pore size and radius of capture for K(+) ions in K-channels. *Sci Rep* 6:19893.
43. Díaz-Franulic I, Sepúlveda RV, Navarro-Quezada N, González-Nilo F, Naranjo D (2015) Pore dimensions and the role of occupancy in unitary conductance of Shaker K channels. *J Gen Physiol* 146:133–146.
44. Chanda B, Asamoah OK, Blunck R, Roux B, Bezanilla F (2005) Gating charge displacement in voltage-gated ion channels involves limited transmembrane movement. *Nature* 436:852–856.
45. Kim GH, Kosterin P, Obaid AL, Salzberg BM (2007) A mechanical spike accompanies the action potential in Mammalian nerve terminals. *Biophys J* 92:3122–3129.
46. Seber GAF, Lee AJ (2003) *Linear Regression Analysis* (Wiley, Hoboken, NJ), 2nd Ed.